Helmholtz-Zentrum
Geesthacht
Zentrum für Material- und Küstenforschung

Final Draft
of the original manuscript:

Chupakhin, S.; Kashaev, N.; Klusemann, B.; Huber, N.:
Artificial neural network for correction of effects of plasticity in equibiaxial residual stress profiles measured by hole drilling
In: The Journal of Strain Analysis for Engineering Design (2017) SAGE

DOI: 10.1177/0309324717696400

Artificial neural network for correction of effects of plasticity in equibiaxial residual stress profiles measured by hole drilling

Sergey Chupakhin[1], Nikolai Kashaev[1], Benjamin Klusemann[1,2] and Norbert Huber[1]

[1]Institute of Materials Research, Materials Mechanics, Helmholtz-Zentrum Geesthacht, Germany

[2]Institute of Product and Process Innovation, Leuphana University of Lüneburg, Germany

Corresponding author:

Sergey Chupakhin, Helmholtz-Zentrum Geesthacht, Max-Planck-Str 1, 21502 Geesthacht, Germany.

Email: sergey.chupakhin@hzg.de

Accepted for publication in the Journal of Strain Analysis for Engineering Design

Abstract

The hole drilling method is a widely-known technique for determination of non-uniform residual stresses in metallic structures by measuring strain relaxations at the material surface caused through the stress redistribution during drilling of the hole. The procedure for solving the inverse problem of determining the residual stresses from the measured strain, the Integral method, relies on calibration data obtained from finite element simulations, assuming linear elastic material behaviour. That limits the method to the measurement of residual stresses well below the yield strength. There is a lack of research regarding effects caused by residual stresses approaching the yield strength and high through-thickness stress gradients of 3000-4000 MPa/mm as well as the correction of the resulting errors. However, such residual stress profiles are often introduced in various materials by processes as laser shock peening, for example to obtain life extension of safety relevant components. The aim of this work is to investigate the limitations of the hole drilling method related to effects of plasticity and to develop an applicable and efficient method for the stress correction, capable of covering a wide range of stress levels. For this reason, the ABAQUS axisymmetrical model was used for simulating the hole drilling process involving plasticity and afterwards the Integral method was applied to the relaxation strain data for determining the equibiaxial stress field. An artificial neural network has been used for solving the inverse problem of stress profile correction. Finally, AA2024 T3 specimens were laser peened and the measured stress fields were corrected by means of the trained network. In order to quantify the stress overestimation in the hole drilling measurement, an error evaluation has been conducted. It is shown that the proposed approach leads to a robust determination even for highly non-uniform stress profiles. This suggests the possibility of applying the hole drilling method to high residual stresses and stress gradients as well, if the presented correction method is applied.

Keywords

Residual stress, hole drilling, effect of plasticity, artificial neural network, finite element analysis, inverse solution

Introduction

The hole drilling method is a well-known technique for measuring residual stresses in metallic structures, which has received much attention over the last thirty years. This is particularly true since it was adapted for determining non-uniform stress fields[1,2,3]. The rising popularity of this method is related to its simple practical realization in many applications, minimal damage to the target specimen, general reliability and acceptable accuracy[4,5]. The hole drilling procedure involves drilling a shallow hole in the specimen, which causes a residual stress redistribution and strain relaxation in the surrounding area of the hole. Optical interferometric measurement techniques are applied for capturing the strain relaxation at the top surface. The residual stress profile is obtained from full-field data of the surface displacement through solving an inverse problem by using analytical techniques such as Fourier analysis, regularization, smoothing and etc.[6,7,8]. However, due to the assumption of linear elastic deformation, the hole drilling measurement is limited to residual stresses of about max. 60-70% of the material yield strength[3,9].

Over the last three decades much research has been accomplished regarding the drilling process[4], surface deformation measurements[10,11], and analytical methods for determining the residual stress profile from the surface displacement data[6,8]. Low-speed drills have substituted electrical discharge machining and electric endmills; and strain gauges have been replaced by optical techniques such as electronic speckle pattern interferometry (ESPI) or Moiré interferometry, which are capable of capturing full-field data about the surface displacement[10-14]. In the 1980s G.S. Schajer[15] proposed finite element calculations for relating the “removed stresses” to the measured strain at the surface, replacing experimentally-determined calibration constants which had been restricted in specimen shape, materials and experimental procedure. Later, Schajer[1,2] developed the Integral method for identification of non-uniform residual stresses from strain relaxations, which substituted the previously applied Incremental Strain and Average Strain methods. Most recently, an advanced numerical approach for calculating stresses from ESPI data has been proposed[8]. The approach allows reducing thousands of displacements to a small number of representative values by utilizing a known mathematical relationship within the measured data. Therefore the Integral method became computationally very efficient and accurate.

Several studies have addressed the problem of the occurrence of plasticity in connection with the hole drilling method, as the residual stresses approach the materials yield strength[9,16-19]. Plastic deformation is the main source of significant errors in the measured stress profiles, due to the violation of the underlying assumption of material linearity in the Integral method. However, proposed solutions are time-consuming and are, in most cases, not applicable for correcting non-uniform residual stress profiles with high through-thickness gradients of up to 4000 MPa/mm. Furthermore, these studies[9,16-18] have only been dealing with few materials, that does not allow the application to the wide range of engineering materials. Therefore, more attention should be paid on developing practical and elegant ways for residual stress correction, covering the full range of stress levels and the relevant range of material behaviours.

One widely known industrial surface modification method for metallic structures is laser shock peening [20]. This process generates deep residual stress fields with strong through-thickness gradients of a magnitude stated above. As a result, the fatigue life of components, treated by laser peening, can be significantly improved[21]. It is worth noting that the stress profiles largely depend on the laser peening parameters as well as the treated material.
The purpose of this study is to investigate the limitations of the hole drilling method related to the effects of plasticity and to develop a method for stress correction. The developed approach employs an artificial neural network, which can be understood as a flexible function that allows approximating any nonlinear relationship between multiple inputs and outputs[22]. The unknown and often complex nonlinear dependency between inputs and outputs is "learnt" from pairs of input-output data, so-called patterns, which are produced e.g. by finite element calculations[23]. For this purpose the hole drilling process was simulated axisymmetrically using ABAQUS[24] including plasticity effects. Afterwards the Integral method was applied to the relaxation strain data using Python programming language[25] for obtaining the desired stress field as function of depth. This procedure was repeated until enough patterns for training and validation of the artificial neural network were gained. Finally, the trained network was applied for solving the inverse problem of stress profile correction.
For demonstration of the applicability of the developed correction method, specimens produced from an AA2024 T3 alloy were laser peened with different parameters and the residual stresses were measured by hole drilling. The proposed approach has been applied in order to correct the measured stress profiles. Moreover, errors have been evaluated in order to provide an impression of the applicability of hole drilling for determination of residual stresses approaching the material yield strength.

Material and Experimental Methods

Material

AA2024-T3 is an advanced aluminum alloy mostly used in aerospace industry, possessing excellent fatigue resistance, high fracture toughness and high formability. Due to its high strength-to-weight ratio AA2024-T3 brings the improvement in damage tolerance of aircraft structures, and is especially used for wing and fuselage structures loaded in tension and also for gears, shafts, bolts and hydraulic valve bodies. The composition of AA2024-T3 consist of wt. 0.3-0.9% manganese, wt. 3.8-4.9% copper, wt. 1.2-1.8% magnesium and silicon, zinc, chromium, lead and bismuth not exceeding a wt. 0.5%[26]. It is a high strength material of adequate workability and has also excellent ductility, which decreases not significantly under strengthening heat treatment[27-29]. Moreover, it has good machinability and surface finish capabilities. It has a density of 2.78g/cm^3 and melting temperature about 500 °C. A T351 temper of AA2024 was performed at a temperature of 410 °C, leading to an ultimate tensile strength of 490 MPa, a yield strength of 370 MPa, a Young's modulus of 73.1 GPa and elongation at break of 16% [30]. The material Vickers hardness is roughly 150 HV 0.2 [30].

Laser shock peening

Laser shock peening is a surface modification technology which is increasingly used for improvement of material properties and targeted microstructure modification. The process induces compressive residual stresses through the depth of the specimen that significantly increases fatigue life in particular when damage is caused by cracks initiated at the surface[21,31]. In comparison with conventional surface modification techniques laser shock peening has the following advantages[32]:

- Flexibility in processing different geometries and capability to be used in existing production lines;
- Low surface roughness;
- Controllable laser pulse beam with the possibility to strengthen the material at the corners;
- Clean process with no need for material recycling, e.g., as for shot peening.

A high energy pulsed laser is used for treating the material surface, which is usually covered by a water-confirming layer. Having passed the water layer, the laser beam is absorbed by the material, turning it into plasma. The plasma expands very rapidly by absorbing the laser energy during the pulse. The water layer transparent for the used laser wave length traps the plasma causing a high pressure at the material surface leading to a shock wave, which propagates into the material. Consecutively, plastic deformations occur as the shock wave pressure exceeds the dynamic yield strength of the material, which leads to compressive residual stresses. In addition, the laser peening process increases the material hardness in the peened area.
Laser shock peening is nowadays well-established for improving resistance to corrosion[20], reducing fretting fatigue damage[32], and increasing resistance to foreign object damage[33]. Possible application area of those improvements to metallic aircraft structures includes fatigue-critical components such as wing attachment fittings, landing gear (including wheels and brakes), fasteners and fastener holes, welded aircraft parts, helicopter components, springs, turbine vanes, and blade bases[34-37]. Compressive stresses are successfully used for the retardation or even complete suppression of fatigue crack formation and the deceleration of crack propagation, thereby enhancing the fatigue life and improving the damage tolerance of light metallic structures[21,34].

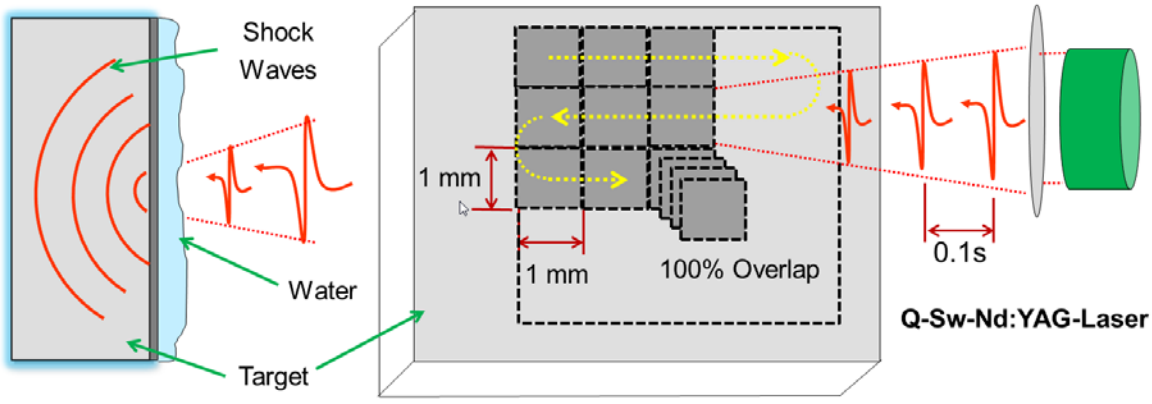

Figure 1. Schematic illustration of the laser shock peening process

In Figure1, the laser peening process is schematically illustrated. The Q-Switched Nd:YAG laser used in this work is capable of working with maximum 10 Hz frequency. The pulse duration can be switched between 10 ns and 20 ns. The material surface was covered with a laminar water layer used as confining medium for the plasma. Specimens produced from AA2024 T3 sheets of 2 mm thickness have been treated with laser pulses sequentially along the path as shown in Figure 1. The laser beam was focused on the surface as square spot using an optical system. Two different optics of 1x1 and 3x3 mm^2 were used in the experiments. For generating very deep compressive stresses up to 5 times 100% overlap of the laser spot was required.

Hole drilling method

Residual stresses generated in the specimens through laser shock peening were measured using the hole drilling system “Prism”. Prism is equipped with an optical electronic speckle pattern interferometer (ESPI) that provides high-quality full-field data for accurate residual stress determination[38].

After drilling a blind hole at the place where the residual stresses should be determined, the surrounding material at the hole immediately relaxes to the new stress equilibrium leading to surface displacements around the hole. For the measurement of these displacements, a laser beam illuminates the specimen surface. Natural roughness leads to diffuse light scattering which is captured by the camera from different angles. In consequence, the camera captures an image consisting of bright and dark spots which is called speckle pattern and is a defined feature of surface topology. The speckle pattern moves as the sample surface is shifting.

Full-field optical data can be compared to thousands of strain gauges at the surface, measuring displacements. Those surface displacements, projected along the sensitivity vector, have an explicit relationship with deviations in the phase angles at the image pixels. Consequently, the Integral method as a means for determining non-uniform residual stress fields from surface relaxations is implemented for solving the inverse task by processing the measured full-field data[1,2,8]. The Integral method calculates residual stresses as function of specimen depth, based on simulation references, expressed as a triangular matrix of calibration coefficients. This matrix consists of many elements typical in the order of 10^3, each of which requires a separate finite element simulation. Essentially, the Integral method solves a system of equations using the least square method, where the solution is a vector of residual stresses at a particular depth.

Following this approach, the Integral method was implemented in [19] for the case of uniaxial residual stress with a linear through-thickness gradient as produced by 3-point bending flexural testing combined with elastic as well as an elastic-plastic FE modelling of the hole drilling procedure. The residual stress profile as a function of depth was determined from the FE simulations which served as virtual hole drilling experiments. By comparing the correct residual stress profile with the results from the elasto-plastic FE analysis, the error in the resulting residual stress was determined. According to statements in the literature, the error was found to be negligible for stress profiles which do not exceed 60% of the yield strength. When the residual stress was exceeding this level, the error increased significantly, up to 21% for a residual stress of 80% of the yield strength. Further

analysis of typical nonlinear laser peening shaped stress profiles with different through-thickness gradients and magnitudes showed errors up to 50% at a depth of 0.2–0.3 mm. Furthermore, the residual stress profiles appeared to be shifted towards larger depths. In was concluded, that the effect of plastic deformation results from the notch effect of the hole. The notch increases the near-surface stress above the yield strength, even though the nominal stress is well below the yield strength. The enhanced plastic deformation in direction of the hole center is interpreted by the Integral method as elastic surface relaxation originating from the "nominal" residual stress profile, leading to a significant overestimation of the residual stress.
Essentially, the approach presented in [19] can be used for determination of the error in the residual stress measurement, and could in principle be applied also for error correction, for instance through an iterative procedure. However, determination of the coefficients for the Integral method for a different material and specimen geometry is time-consuming. Therefore, a more general correction approach is needed for the determination of the residual stress profiles generated by laser peening, covering the relevant range of residual stress levels and profiles as well as material behaviors.

Computational methods

Finite element modeling

Schajer[15] has proposed a finite element model for the simulation of the hole drilling process, where the loading is applied externally to the curved surface of the hole with opposite sign to the original stresses, leading to strain relaxations at the top surface of the specimen. Following the assumption that residual out-of-plane, normal, and shear stresses are negligible and all free surfaces are unstressed, the finite element model is simplified towards a two-dimensional axisymmetric problem for simulation of equal biaxial stress distributions corresponding to laser peening induced stress fields.
MSC Patran 2012.2[39] and ABAQUS 6.13-1[24] were employed as pre-processor and solver, respectively. The Integral method was implemented in Python[25]. The finite element mesh of this model, shown in Figure 2, consists of 5985 elements. Axisymmetric bilinear quadrilateral elements CAX4 were used. The mesh discretization on the top surface was adjusted according to the resolution of the full-field surface displacement data of the camera of the hole drilling system "Prism".
The mesh had to be modified for introducing the hole. This was realized by removing elements within given hole boundaries for each depth increment of the drilling process using Python. A fine mesh size of 0.025 mm (square elements) was applied in the area surrounding the hole, and a mesh size of 0.1 mm was used near the far boundaries. The mesh size was gradually decreased from the hole towards the boundaries using the Patran transition triangular option. The maximal hole depth is 1 mm, and the hole diameter 2 mm. Simulations were performed for each increment of a given hole depth. In total, 10 equally spaced increments were used along the depth. The height of the model is 2.5 mm, and the far boundary diameter 6 mm.

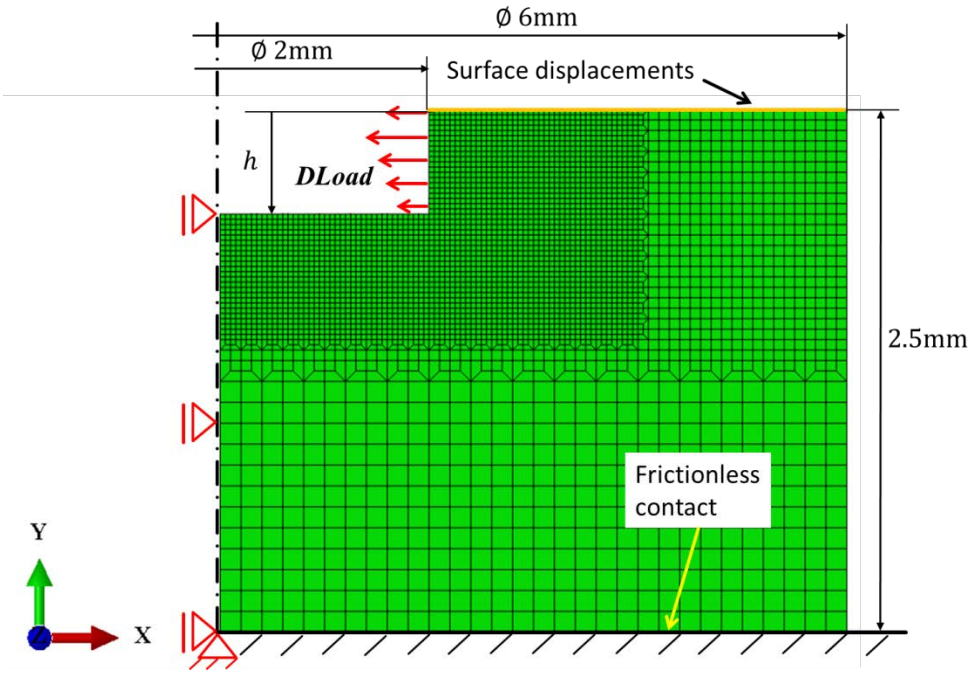

Figure 2. Finite element mesh used for the simulations.

The *DLoad* subroutine of ABAQUS was used for applying the load to the hole surface, which defines the laser peening shaped stress profile, mathematically described according to Equation (9), normal to the surface. The nodes at the bottom of the model are restricted to move down in vertical direction due to the frictionless ground, while those at the symmetry axis are fixed in horizontal direction. Moreover the left bottom node is restricted vertically to prevent the body movement.

An isotropic strain hardening plasticity model was used in all simulations; hence, Young's modulus E, Poisson's ratio v, yield stress σ_y and the hardening curve define the material properties. Isotropic hardening implies that the yield surface changes size uniformly in all directions such that the yield stress increases in all stress directions as plastic straining occurs. The von Mises yield criterion with isotropic hardening was used. The relationship between the residual stresses and the strain relaxations was obtained through separate simulations and was stored as a relaxation matrix.

Neural Networks

Artificial neural networks are computational tools developed on the basis of the interconnection of the neuron in the nervous system of the human brain[22]. They represent a type of non-linear processing that is ideally suited for tasks where the solution does not exist as closed form relationship. The neural network can be trained to approximate any kind of nonlinear relationship using a training algorithm and sample data consisting of so-called patterns. In the past two decades neural network has been successfully applied for solving complex direct problems aiming at prediction or analysis[40] as well as inverse problems, typically dealing with the identification of mechanical properties[41-49]. In the following, only a brief description of neural network is given.

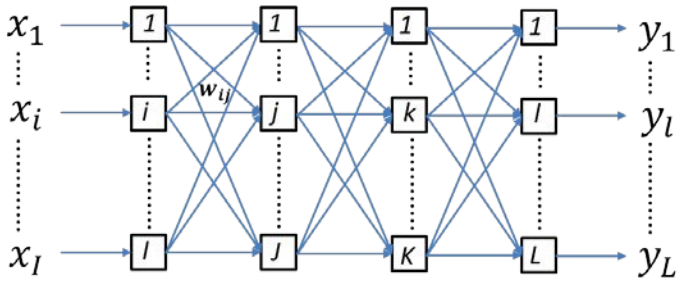

Figure 3. Sketch of a multilayer feedforward neural network after Huber, Tsakmakis[47].

In Figure 3 a sketch of a hierarchical neural network is shown. It consists of neurons connected with links to a highly parallel structure. The first and last layer serves as input and output layer, respectively, where the corresponding data are collected in the vectors $\boldsymbol{X} = (x_1, x_2, \dots, x_I)^T$ and $\boldsymbol{Y} = (y_1, y_2, \dots, y_L)^T$.
The two main features of hierarchical neural networks as they are used in this work can be summarized as described by Yagawa and Okuda[40]:

- One can automatically construct a nonlinear mapping from multiple input data to multiple output data in the network through a learning process of some or many sample input vs. output relations.
- The network has a capability of so-called "generalization", i.e. a kind of interpolation, such that the trained network estimates appropriate output data even for unlearned data.

In general, the training is performed by minimizing the value of an error function

$$E = \sum_{n=1}^{N} \sum_{l=1}^{L} \left(d_l(n) - y_l(n)\right)^2 + 10^{-\alpha} \sum w_{ij}^2, \tag{1}$$

where d_l is the desired output and y_l is the calculated output at unit l for a certain pattern n. The left part represents the error of the L outputs and all N patterns, while the right part is the norm of the weight vector. The network generalization is reached by minimizing E, which is obtained through adjusting the output error and the synaptic weights w_{ij} as small as possible in each learning iteration (one epoch).
The training code provides an error measure denoted by MSE in order to compare the quality of different neural networks during training that can also be used for visualizing training and generalization properties:

$$MSE = (10^3/NL) \cdot \sum_{n=1}^{N} \sum_{l=1}^{L} (d_l(n) - y_l(n))^2, \tag{2}$$

The number of patterns N depends on the complexity of the problem and type of pattern set (training or validation). MSE values for training and validation patterns are comparable, i.e. $MSE_T \sim MSE_V$, when the neural network provides good generalization.
The absolute value of the relative error

$$err_l = |e_l/d_l| = |(d_l - y_l^N)/d_l|, \tag{3}$$

has been introduced in order to analyze the error distribution of the identified values for all patterns, where l denotes the output unit. Also for an output quantity y_l, we denote the confidence interval by err_l 90% which is defined as the err_l containing 90% of all training patterns.

Application of neural network to residual stress profiles

Identification of residual stress profile

Neural network generation

The identification of the correct residual stress profile from measured data requires the solution of a complex inverse problem by including prior knowledge about the elastic-plastic material behavior. The flowchart of the approach of this work is illustrated in Figure 4. In a first step, patterns are generated by solving the direct problem using the FEM method and integral method, simulating the hole drilling experiment and residual stress measurement (for more details about this step, see [19]) for varying materials and residual stress profiles. The resulting patterns, consisting of pairs of "measured" residual stress profiles from the Integral method and predefined residual stress profiles, form the training basis for the artificial neural network. The known material behavior serves as additional input which is needed for determining the amount of correction. Once the network has been trained in the second step for approximation of the general relationship between the presented patterns, it can be applied for correcting residual stress profiles that were not used for training, for example data from experiments.

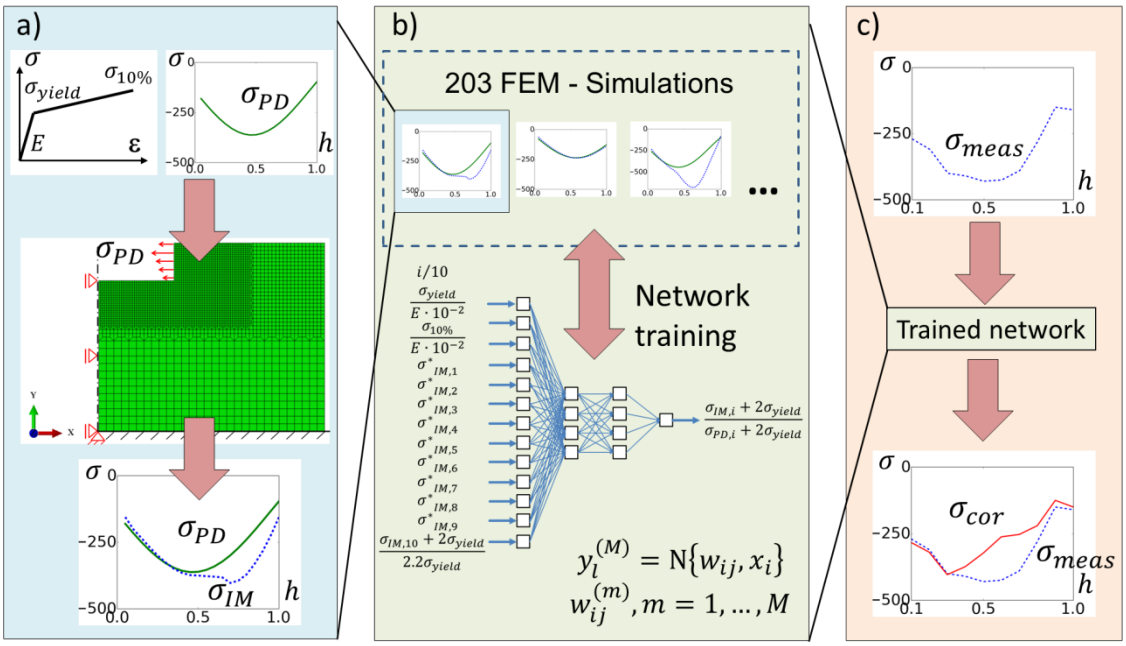

Figure 4. Flowchart of neural network application a) pattern generation using FE simulations; b) training of the network; c) application of the network to experimental data.

For the generation of training patterns the finite element model described above was used for all simulations. The experimental validation of the model and its predictive capability with three point bending tests is presented in a previous study[19]. For each new pattern, material parameters and residual stress profiles were randomly chosen within predefined intervals to produce a sufficient number of independent training patterns, covering mainly the relevant region where effects of plastic deformation are expected to become important. A compressive non-linear residual stress profile was expressed as a trigonometric function, which sufficiently describes typical shapes introduced by laser shock peening[32]. The subroutine *DLoad* was used in ABAQUS for applying such residual stresses using the equation

$$\sigma_{PD}(h) = \sigma_0\big(k_0 - \sin\big(k_1\pi(h - h_0)\big)\big)\,, \tag{4}$$

where $\sigma_{PD}(h)$ is the predefined compressive stress at the depth of h in the material, k_0 and h_0 shift the stress profile on the stress axis and depth, respectively. The parameters σ_0 and k_1 are used for scaling the stress profile along the stress axis and the depth, respectively. Limiting values of profile coefficients included in Eq. (4) and material properties are listed in Table 1, where σ_{yield} is the yield strength, E is the Young's modulus, and $\sigma_{10\%}$ is the true stress at a true plastic strain of 10%. With these limits, a wide range of materials and residual stress profiles is covered, that may occur in technical applications, such as life extension of aircraft components.

Table 1: Minimum and maximum values for profile coefficients and material properties used for generation of training and validation patterns. σ_{yield} is the yield strength, E is the Young's modulus, $\sigma_{10\%}$ is the true stress at a true plastic strain of 10%.

	σ_0, MPa	k_0	k_1, mm^{-1}	h_0, mm	σ_{yield}, MPa	$\sigma_{10\%}$, MPa	E, GPa
Min	150	- 0.3	0.7	- 0.2	300	400	70
Max	360	- 0.9	1.3	0.2	500	600	210

A consistent presentation of the patterns for training and later application of the neural network requires the introduction of definitions which serve for translating the relevant data into the input vector $\boldsymbol{X}$ and output vector $\boldsymbol{Y}$ (see Fig. 4). An appropriate choice of input and output definitions supports the capability of the network for improved generalization and higher accuracy. For details about the application of dimensional analysis and the incorporation of prior knowledge we refer to literature[42-49]. Generally, there exist many possibilities in combining the different independent and dependent quantities in linear independent dimensionless quantities that again are included in the input and output definitions. How many of them are needed, depends on the complexity of the problem and the robustness of the inverse solution with respect to scatter. Generally, a lower number of

inputs reduces the complexity of the neural network and enhances the generalization while a higher number of inputs can help to improve the robustness. The latter results from the circumstance, that adding inputs of the same type (e.g. a larger number of stress values over depth) helps the network to identify the general trend, independent from individual scatter of the data points. The final input and output definition of a properly working neural network is typically the result of an extensive study that compares different possibilities in view of the desired performance.

In what follows, a discretization of the depth of the form $h(i)/h_{ref} = i/10$ is applied, where the reference depth is the maximum depth applied for the hole drilling simulation, $h_{ref} = 1\text{mm}$. The residual stress profile is represented by the respective values obtained at depths $h(1)$ to $h(10)$. The residual stress at the depth of h_{ref} is chosen as reference and is used for normalization of the residual stress profile up to this depth.

In general, the residual stress profile can include a transition from compression to tensile stress. It is convenient to shift the stress profile by adding two times the yield stress. This ensures that all stress values are sufficiently positive and avoids division by zero or by very small stress values during normalization. As resulting dimensionless quantity, the shifted and normalized residual stress is defined as

$$\sigma^*_{IM,i} := \frac{\sigma_{IM,i} + 2\sigma_{yield}}{\sigma_{IM,10} + 2\sigma_{yield}}, \tag{5a}$$

$$\sigma^*_{PD,i} := \frac{\sigma_{PD,i} + 2\sigma_{yield}}{\sigma_{PD,10} + 2\sigma_{yield}}, \tag{5b}$$

where $\sigma_{\mathrm{IM,i}}$ is the residual stress obtained by applying the Integral method (IM) to simulation data, i.e. without correction of effects of plastic deformation, at a depth of $h(i)$. The predefined (PD) residual stress profile, which was used as input to the FEM simulation, is translated to the dimensionless quantity $\sigma^*_{PD,i}$ in the same way as $\sigma^*_{IM,i}$, according to Eq. (5b). The values $\sigma^*_{PD,i}$ represent the desired stress profile, to which the values $\sigma^*_{IM,i}$ shall be corrected by the neural network.

For the creation of input and output definitions, elastic and plastic material properties (Young's modulus, E, yield stress, σ_{yield}, and stress at plastic strain of 10%, $\sigma_{10\%}$) as well as the residual stress profiles $\sigma^*_{PD,i}$ and $\sigma^*_{IM,i}$ are combined in dimensionless quantities. In addition to the information about the residual stress profile $\sigma^*_{IM,i}$, one more dimensionless quantity is required that relates the reference value of the residual stress profile, $\sigma_{IM,10}$, to the mechanical properties represented by the yield stress, e.g. in form $(\sigma_{IM,10} + 2\sigma_{yield})/(2.2\sigma_{yield})$. The factor 2.2 in the denominator is derived from the range of the patterns and scales this input to the order of 1.

The three material parameters are combined in two further dimensionless quantities by normalizing the two flow stresses to the Young's modulus. For better comparison of the different inputs, also here the division of the Young's modulus by a factor of 100 brings the order of the input quantities to a similar level. Such scaling has no further effect on the performance of the neural network but can help to visually check the large amount of patterns with regard to correct data processing. As final input, the depth is given, at which

the correction factor for the residual stress shall be determined. Based on these considerations, the following input and output definition was found:

$$\boldsymbol{X} := \left\{\sigma^*_{IM,1}, \sigma^*_{IM,2}, \dots, \sigma^*_{IM,9}, \frac{\sigma_{IM,10}+2\sigma_{yield}}{2.2\sigma_{yield}}, \frac{\sigma_{yield}}{E\cdot 10^{-2}}, \frac{\sigma_{10\%}}{E\cdot 10^{-2}}, \frac{i}{10}\right\}, \tag{6}$$

$$\boldsymbol{Y} := \left\{\frac{\sigma_{IM,i}+2\sigma_{yield}}{\sigma_{PD,i}+2\sigma_{yield}}\right\}, \tag{7}$$

After training of the network to patterns consisting of pairs $(\boldsymbol{X}, \boldsymbol{Y})$ the neural network finally approximates the function

$$\left(\frac{\sigma_{IM,i}+2\sigma_{yield}}{\sigma_{PD,i}+2\sigma_{yield}}\right) = f\left(\sigma^*_{IM,1}, \dots, \sigma^*_{IM,9}, \frac{\sigma_{IM,10}+2\sigma_{yield}}{2.2\sigma_{yield}}, \frac{\sigma_{yield}}{E\cdot 10^{-2}}, \frac{\sigma_{10\%}}{E\cdot 10^{-2}}, \frac{i}{10}\right), \tag{8}$$

For obtaining the corrected residual stress, the ratio $\frac{\sigma_{IM,i}+2\sigma_{yield}}{\sigma_{PD,i}+2\sigma_{yield}}$ obtained from the network is solved with respect to the absolute values $\sigma_{PD,i}$, which represent the predefined, but in the application unknown residual stress profile in the specimen. Because the trained neural network is able to interpolate between presented patterns, the output definition is in the application of the network not restricted to the depth increments that were used for training. This means, that the last input parameter in Eq. (6), which is $i/10$, can be generalized to a variable h/h_{max}, continuously scanning the depth range between 0.1mm and 1mm.

The structure of neural network is defined by thirteen input neurons, two hidden layers, each consisting of four neurons, and one output neuron. It has been trained with 2030 patterns for 5000 epochs without any sign of overlearning. The training patterns were built from 203 FEM simulations, where every set of 10 patterns had 12 identical input neurons and only the 13th input, which represents the depth h, was varying within these ten patterns from 0.1 to 1.0.

Identification quality of the neural network

The best generalization had been achieved by training with $\kappa = 6.0$, balancing the absolute value of the synaptic weights in relation to the training error and thus avoiding overlearning (see Eq. (1)). 1827 out of 2030 patterns were used as training patterns and 203 were randomly selected for validation from within the training range, i.e. none of the validation patterns belonged to the boundary enclosing the patterns. Corresponding to Equations (2) and (3) comparable mean error values of $MSE_T = 2.2*10^{-5}$ and $MSE_V = 2.5*10^{-5}$ from training and validation were, respectively. Very low relative errors within a 90% confidence interval of err_Y^T = 1.57% and err_Y^V = 1.58% were achieved for training and validation patterns, respectively. The resulting quality after training of the neural network over 5000 epochs is presented in Figure 5. It illustrates in addition to the given error measures that the neural network can predict the data for untrained patterns with the same quality as the training patterns indicating a high level of generalization.

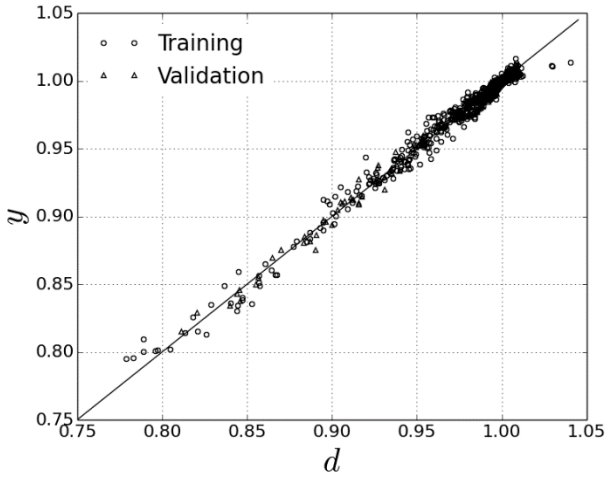

Figure 5. Identification quality of the neural network, presented by calculated output y vs. desired output d according to the definition in Eq. (1)

Verification of the identification network for AA2024-T3 and different residual stress profiles

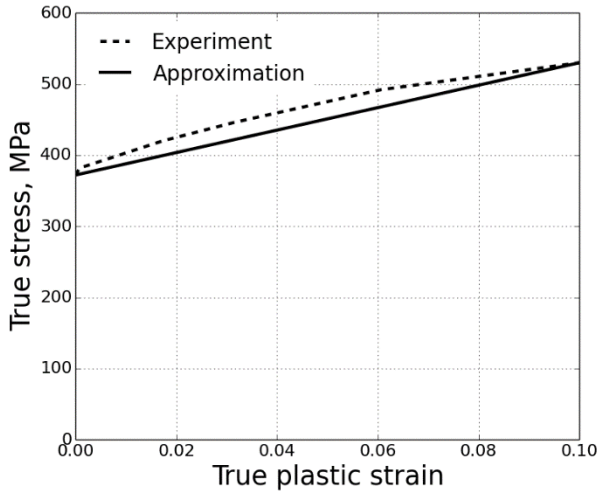

Figure 6. True stress-plastic strain curve for material hardening of AA2024-T3.

For further inspection of the performance of the neural network, four randomly chosen residual stress profiles have been simulated with the material parameters for AA2024. The parameters serve for testing the trained neural network using patterns which were not involved in the training process. This additional verification implements basically a similar procedure as validation patterns during learning. However, now its capability is tested with regard to the absolute values obtained for the corrected residual stress profile. The true stress-plastic strain curve of AA2024 was obtained from experimental tensile test data[30]. The nonlinear work hardening was approximated with a linear segment as shown in Figure

6 in accordance to the definition in training patterns. In order to check for a possible sensitivity of the neural network with regard to this simplification, both the nonlinear stress-plastic strain curve and its linear approximation were tested. The excellent agreement of the two corrected profiles confirmed, that the proposed linear approximation sufficiently describes the elastic plastic material behaviour.

The validation examples for an increasing ratio of residual stress to yield strength $\sigma_{PD,max}/\sigma_{yield}$ are shown in Figure 7(a)-(e). The predefined residual stress profiles applied in the hole drilling simulations (dotted curve), the data obtained from the Integral method (dashed curve) and the corrected profiles obtained through the neural network (solid curve) are displayed. In Table 2 maximum ($\Delta\sigma_{max}$) and mean absolute errors ($\Delta\sigma_{avg}$) are summarized for simulated (Integral method) and neural network corrected residual stress profiles in relation to the predefined ones. The coefficients of the predefined residual stress profiles according to Eq. (4) are listed in Table 2 as well.

The compressive stress profile shown in Figure 7(a) with a maximum of 60% of the yield strength (here approximately at a depth of 0.6 mm) does not require a correction, confirming the conventional validity limit of the Integral method also for the laser peening profile. The mean absolute errors for both simulated and corrected profiles are within the deviation range of the Integral method, but even in this case, the network further reduces the error by more than half. In the case of negligible effect of plastic deformation the neural network is trained to deliver a correction factor of 1.0, i.e., the neural network can be applied to any measurement data even if a correction is not required.

The simulated stress curves in Figures 7(b)-(e) demonstrate growing deviations between the predefined and simulated profiles with increasing ratio of residual stresses versus yield strength. It can be concluded that the effect of plasticity is strongly dependent on the combination of the shape of the predefined stresses and the depth where the peak values occur. The simple assumption about the applicability of the hole drilling for measurement of residual stresses not exceeding 60% of the yield strength, as it is found in literature[3,9], should be improved by considering the shape of the stress profile as well.

The correction by the neural network leads to a strong reduction of the error resulting from the Integral method. In all cases the mean absolute errors do not exceed 10 MPa, showing the ability of the neural network for correcting also “unseen” patterns with the same accuracy as it has been achieved for the training patterns. The corrected stress values are close to the predefined stresses along the whole depth and without any specific bias. The remaining deviations are due to the approximate nature of the neural network.

The stress profile shown in Figure 7(e) is doubtfully achievable by means of laser shock peening for AA2024 but can give an impression about the possible deviation in stress determination and demonstrates the inapplicability of hole drilling without correction in such cases. For this case the neural network reduces the maximum deviation from 306 MPa to 21 MPa, making it of the magnitude of an error practically accumulated from the other sources of inaccuracy of the hole drilling measurement.

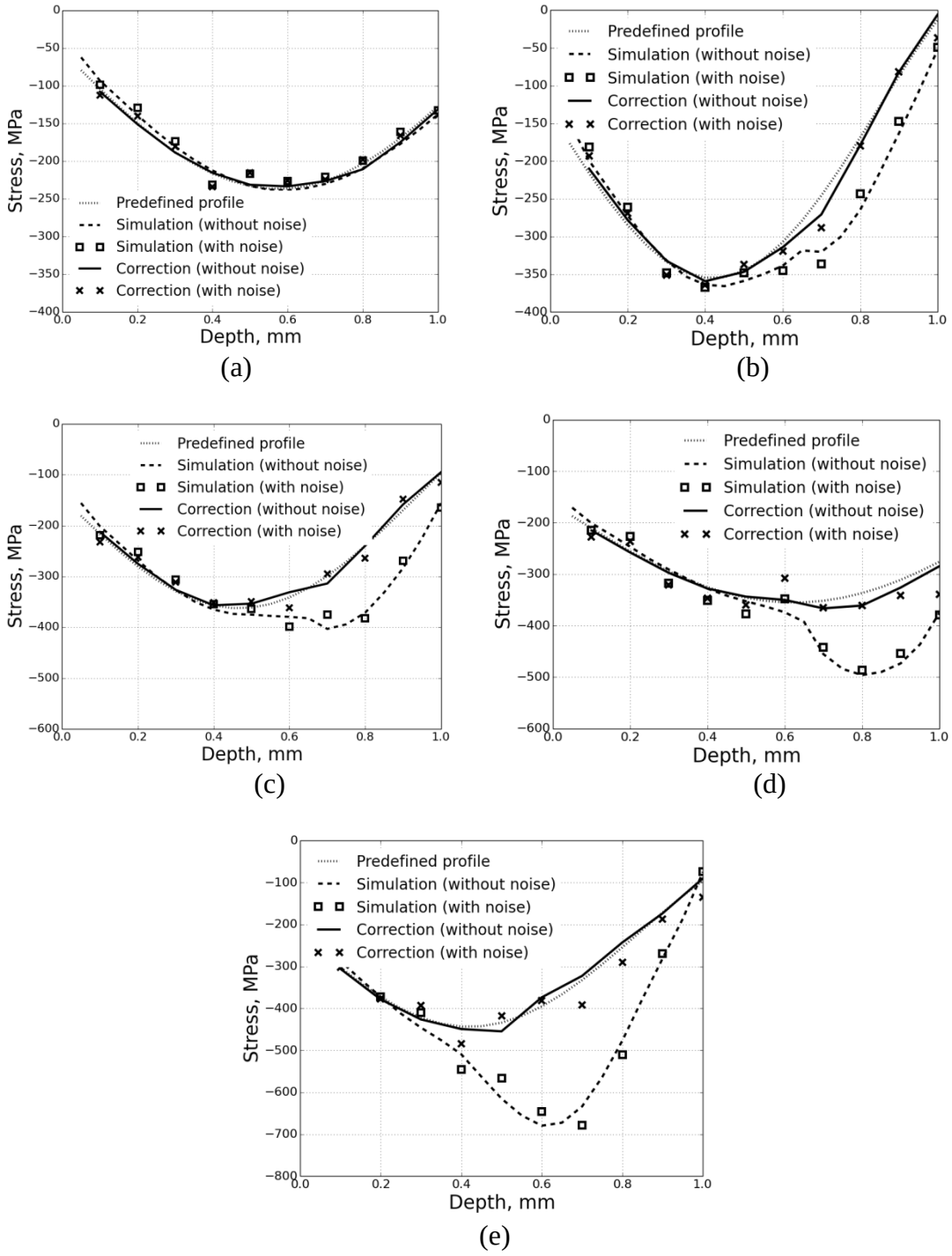

Figure 7. Validation samples for prediction of predefined stress profiles by neural network for increasing ratio of maximum residual stress to the yield strength a) $\sigma_{PD,max}/\sigma_{yield}$ = 60%, b) $\sigma_{PD,max}/\sigma_{yield}$ = 92%, c) $\sigma_{PD,max}/\sigma_{yield}$ = 95%, d) $\sigma_{PD,max}/\sigma_{yield}$ = 95%, e) $\sigma_{PD,max}/\sigma_{yield}$ = 116%

Table 2: Predefined stress profiles and errors of simulated and neural network corrected stress profiles in relation to the predefined stress profiles.

#	Predefined profile					Simulation (Integral method)		Correction (network)	
	σ_0, MPa	k_0	k_1, mm^{-1}	h_0, mm	$\frac{\sigma_{PD,max}}{\sigma_{yield}}$, %	$\Delta\sigma_{max}$, MPa	$\Delta\sigma_{avg}$, MPa	$\Delta\sigma_{max}$, MPa	$\Delta\sigma_{avg}$, MPa
(a)	182.2	- 0.30	0.87	- 0.08	60	17.2	6.6	7.3	2.9
(b)	219.2	- 0.62	1.19	0.06	92	96.0	37.0	25.0	7.4
(c)	218.4	- 0.66	1.07	0.03	95	131.5	49.2	14.7	5.8
(d)	192.0	-0.85	0.82	0.02	95	164.8	55.4	21.5	10.0
(e)	223.1	- 0.88	1.19	- 0.03	116	306.0	123.2	20.8	8.0

In conclusion, it can be stated that the proposed choice of the dimensionless quantities for inputs and outputs satisfactorily fulfils the given objectives. Since the neural network is trained by patterns covering a large range of materials and residual stress distributions, it is designed to be applicable to a large range of experimental data. For the application of the neural network only a few material properties σ_{yield}, $\sigma_{10\%}$, E have to be known. Based on these properties the measured stress profiles can be effectively corrected as demonstrated in Figure 7(a)-(e). In case of pure elastic deformations the neural network will keep the measured profile within the accuracy of the Integral method. Therefore the method is applicable without experimentator's prior knowledge of plasticity occurrence.

Sensitivity of the neural networks to noise

The previous section leads to the conclusion that the neural network can be used for the correction of measured residual stress profiles with an accuracy which is comparable to the Integral method, when the input data are provided by simulations and can be considered to be exact. However, every experiment includes measurement uncertainties and scatter; finite element simulations have uncertainties relating to capturing all relevant effects of the experiment such as the boundary conditions or large displacement formulation.
It can easily happen particularly when solving inverse problems that neural networks which are trained by accurate model data are very sensitive to scatter, as they potentially have successfully learned to interpret highly accurate signals from the different inputs. Such networks can predict meaningless results for experimental data, where scatter is interpreted as a real effect and is translated with corresponding magnification to the output.
For this reason, all finite element simulations from the previous section were used to generate new patterns, where random noise $\Delta\sigma_{IM}$, varying between -10% and 10% of the original data with equal probability, was artificially added to the simulated stress values σ_{IM} . A neural network with the same structure as well as input and output definition as described in the previous section has been trained by these patterns. The achieved accuracy after training 5000 epochs is as follows: the mean error values for training and validation are $MSE_T = 1.1*10^{-4}$ and $MSE_V = 1.6*10^{-4}$; the absolute relative error values within 90% confidence intervals are err_Y^T = 3.48% and err_Y^V = 3.90%. The presence of an artificial

noise of 10% in the predefined patterns has increased training and validation errors approximately by a factor three. This means that the performance of the neural network is reduced by uncertainties, but it is still capable of fulfilling its task with an accuracy which is better than 5% for more than 90% of the patterns.

Verification of the identification network for AA2024-T3 and "noisy" residual stress profiles

In order to demonstrate the robustness of the network, the same validation cases were chosen as described in Table 2, but now artificial scatter was added to the values $\sigma_{IM,i}$, as described for the training patterns. The residual stress values $\sigma_{IM,i} + \Delta\sigma_{IM}$ used for the neural network input are included in Fig. 7 as markers (squares), scattering around the dashed curve. The results from the neural network correction are added in Fig. 7(a)-(e) (cross markers). They demonstrate an overall good correction of the "noisy" stress profiles implying that the network is able to extract the relevant information from the redundant input data providing the information about the residual stress profile. However, the applied noise is transferred to the corrected profile through the normalization of the neural network output according to Eq. (7). Thus, the corrected stress values also scatter around the predefined stresses, but without any bias so one can apply an interpolation technique to obtain the smooth corrected curve.

The errors of simulated and corrected stress profiles are presented in Table 3 together with the errors from the previous section (without artificial scatter). By applying the neural network to the "noisy" residual stress profiles both maximum ($\Delta\sigma_{max}$) and mean absolute errors ($\Delta\sigma_{avg}$) of the corrected profiles were increased by the factor of 1.5 to 4.0 which is of same magnitude as the absolute errors err_Y^T and err_Y^V growth for training and validation patterns, respectively. The increase of the correction errors mimic the measurement uncertainties typically encountered by hole drilling. In case of negligible plastic deformations the neural network still maintains the stress curve unchanged, even though the correction errors remained almost the same due to the introduced noise, which means that the artificial scatter with the factor of 1.0 was translated into the corrected data (Fig. 7(a)). Also with added scatter, the effect of plasticity has been mitigated with an accuracy that is comparable to the accuracy of the hole drilling method described in the experimental methods part. From our own experimental observations this accuracy is approximately 30 MPa.

Table 3: Errors of simulated (Integral method) and corrected stress profiles (network) with and without additional noise for different predefined residual stress profiles.

#	Simulation (IM) without measurement uncertainties		Simulation (IM) with measurement uncertainties		Correction (network) without measurement uncertainties		Correction (network) with measurement uncertainties	
	$\Delta\sigma_{max}$, MPa	$\Delta\sigma_{avg}$, MPa	$\Delta\sigma_{max}$, MPa	$\Delta\sigma_{avg}$, MPa	$\Delta\sigma_{max}$, MPa	$\Delta\sigma_{avg}$, MPa	$\Delta\sigma_{max}$, MPa	$\Delta\sigma_{avg}$, MPa
(a)	17.2	6.6	21.0	10.5	7.3	2.9	18.9	9.4

(b)	96.0	37.0	103.5	43.7	25.0	7.4	40.8	20.7
(c)	131.5	49.2	150.0	51.4	14.7	5.8	31.1	16.8
(d)	164.8	55.4	139.3	50.2	21.5	10.0	50.9	21.1
(e)	306.0	123.2	339.2	126.5	20.8	8.0	56.1	34.3

Application to measured laser shock peening residual stress fields

In order to see, how the neural networks presented in the previous sections react to real experimental data, both solutions are applied to correct the measured residual stress profiles. Laser shock peening has been applied to AA 2024T3 2 mm thin specimens with the material parameters given in the material's section. The residual stress profiles shown in Figure 8(a)-(c) were achieved using the laser peening parameter sets given in Table 4.
The laser pulse duration of 20 ns was used in all experiments. In case of using the 3 mm optics, the peened square area was 15 mm by 15 mm, which was covered by 25 laser pulses. For the 1mm optics, the treated area was 5 mm by 5 mm covered by 25 laser pulses. As can be seen in Figure 8(a)-(c) deeper compressive residual stresses were induced by using 1mm optics and large amount of overlap and the maximum value of compressive stress is also increased. Every parameter set was replicated 3 times in order to increase the process reliability. The holes were incrementally drilled at the center of the treated area using a drill diameter of 2 mm until a maximum depth of 1mm, which is half the thickness of the specimens. The obtained three residual stress profiles for each laser peening parameter set were averaged before correction.
The averaged stresses and the material properties were used to feed the trained neural network for the correction of potential plasticity effects. Two cases were investigated. In the first case, the stress profiles are assumed to be "ideally" measured and the neural network without additional noise was used. In the second case, the same stress profiles were assumed to be measured with uncertainties; therefore the neural network that has been trained with additional scatter was applied. For each residual stress profile, the dimensionless input quantities were calculated according to the input definition given in Equation (7). Afterwards the neural networks were used to provide the correction factor for the residual stress as a function of depth h. The results are illustrated in Figure 8(a)-(c). From the comparison of the results for both neural networks it can be seen, that the network that has been trained without artificial scatter is similarly robust when applied to experimental data, thanks to the redundant input of the residual stress profile in form of nine $\sigma^*_{IM,i}$ values.

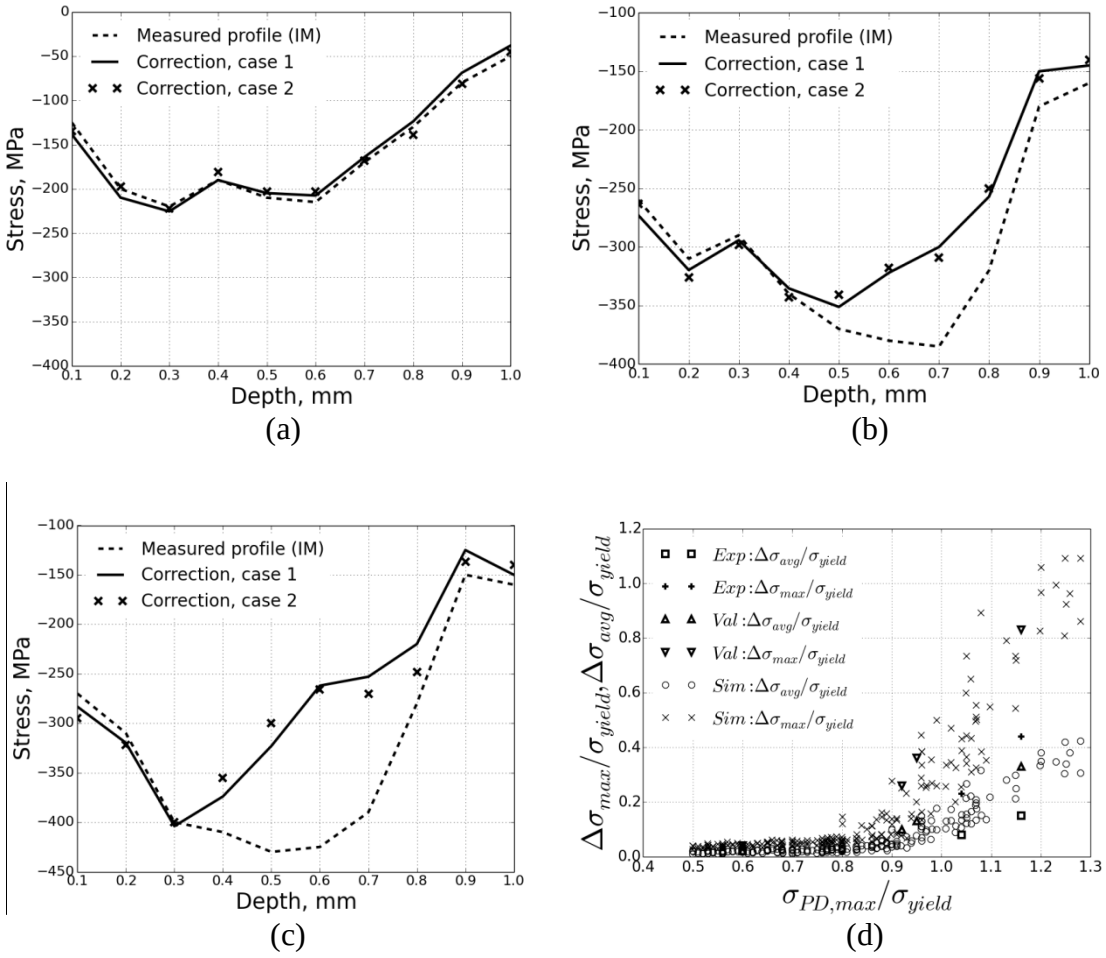

Figure 8. Correction of laser peening induced stress profiles by the neural network a) $\sigma_{cor,max}/\sigma_{yield}$ = 60%, b) $\sigma_{cor,max}/\sigma_{yield}$ = 104%, c) $\sigma_{cor,max}/\sigma_{yield}$ = 116%; d) Normalized maximum error ($\Delta\sigma_{max}/\sigma_{yield}$) and mean absolute error ($\Delta\sigma_{avg}/\sigma_{yield}$) versus the stress factor ($\sigma_{PD,max}/\sigma_{yield}$) for all FE patterns (circles, crosses, triangles) and measured laser peening residual stress profiles.

Table 4: Laser shock peening parameters and the errors of measured stresses in relation to corrected stresses by neural network

	Measured (Integral method) without uncertainties		Laser peening parameters		
	$\Delta\sigma_{max}$, MPa	$\Delta\sigma_{avg}$, MPa	Pulse energy, J	Optic system	Overlapping, number of shots
(a)	13.4	7.7	5	3 mm	2
(b)	85.2	30.1	5	1 mm	2

(c)	163.3	56.9	5	1 mm	5

In Figure 8(a) the measured stress values are lower than 60% of the yield strength. As expected, no corrections were needed in this case and the neural network with and without measured uncertainties reproduce the original profile. The mean absolute error of 7.7 MPa is within the tolerance of the Integral method.
In Figures 8(b)-(c) the stress profiles were corrected towards the lower compressive values, which indicates the presence of plastic deformation, causing the stresses to be overestimated. It should be noted that the subsurface values in the depth interval 0.1 to 0.3 mm were not corrected by the neural network at all. This is analogous to the training patterns. It can be seen that the more the measured stresses approach or even overcome the yield strength the larger the corrections have to be, leading to an increase of the mean absolute errors. The maximum corrections of 85.2 MPa and 163.3 MPa, illustrated in Figures 8(b) and (c), respectively, are applied at the depth range 0.6-0.7 mm, where the maximum values of the measured stress profiles are located. Therefore, the correction is essential to the residual stresses of such a magnitude.
In Figure 8(d) the normalized maximum errors ($\Delta\sigma_{max}/\sigma_{yield}$) and mean absolute errors ($\Delta\sigma_{avg}/\sigma_{yield}$) are plotted versus the stress factor $\sigma_{PD,max}/\sigma_{yield}$ for all training and validation patterns as well as for the corrected laser peening residual stress profiles. One can see that the normalized errors are within 8% as long as the stress factor is $\sigma_{PD,max}/\sigma_{yield} \leq 0.8$. Therefore, our analysis reveals, that – in extension to the commonly assumed 60% limit – the hole drilling method can be reliably used for measuring the laser peening shaped residual stress profiles up to 80% of the yield strength. Beyond this value, the error grows progressively and reach maximum values of 43% and 110% for $\Delta\sigma_{avg}/\sigma_{yield}$ and $\Delta\sigma_{max}/\sigma_{yield}$, respectively, at $\sigma_{PD,max}/\sigma_{yield}$ of approx. 1.3. The errors' scatter reflects the amount of correction that depends on the shape of the residual stress profile. From the increasing width of the scatter band shows that the relevance of the profile shape gains in importance with increasing stress level $\sigma_{PD,max}/\sigma_{yield}$. Concerning the experimental stress profiles, presented in figure 8(b)-(c), it can be seen that they are located at the lower boundary of the scatter bands in Figure 8(d) (squares and pluses). This confirms that the experimental laser peening profiles, analyzed in this work, are well within the range of residual stress profiles, covered by the neural network.

Conclusions

The Integral method has been enriched through an elastic as well as an elastic-plastic finite element modelling for the given specimen geometry in order to solve the inverse problem of residual stress determination from surface relaxations. The parameter ranges for the simulations are selected to cover the relevant range of material behaviour and residual stress profiles for typical experimental applications. An artificial neural network was used to identify the relationship between predefined ("actual") and simulated stress profiles (plastically affected data obtained from the Integral method), through training with more than 2000 patterns built from the simulation data. It was shown with the help of the network correction that the hole drilling method can be applied to residual stress profiles that exceed

the conventional limit of validity of this method by almost a factor of two. Finally, laser peening induced residual stress profiles were corrected by the trained neural network to show the applicability of the method to experimental data.
The main advantage of usage of an artificial neural network is its generalization capability, i.e. the ability of a trained network to predict appropriate output data for unlearned data. The trained neural network has shown degree of accuracy comparable to the conventional Integral method in the valid application range, even when artificial noise is present.
It is worth to note that the stress errors strongly depend on the stress profile shape and its magnitude which requires a sophisticated correction method. Unlike in the recent studies[9,16-18], the novelty of this work lies in the practical and elegant way to correct any non-uniform through-thickness stress profile for any type of material within the given parameter range of training patterns. The neural network needs to be trained with simulation data only once, and then can be used for stress correction of residual stress profiles with no need of caring for validity limits concerning the magnitude of residual stress related to the yield stress. The method can be easily adapted for correction of residual stresses generated through other sources of metal treatment than laser shock peening such as the shot peening or the hammer hardening, by including the occurring patterns, which carry the information about the typical profile shapes and treated materials.
However, the proposed approach still has a limitation. In this study the specimen thickness and the driller diameter were kept 2.5 and 2 mm, respectively. Schajer et al.[50] have investigated the linear-elastic behaviour of the specimen during the hole drilling in dependence on hole depth to the thickness ratio, and observed a significant error in stress determination when the maximum hole depth exceeds half of the specimen thickness, which is now declared in the ASTM E837-13a standard[51]. Additionally the hole depth should be smaller than the hole radius. The stress error is caused by the additional bending to which the specimen is subjected. The presence of plasticity may strengthen this effect leading to an increase of measurement errors. Therefore future research should also consider an extension of the presented method by including a general specimen thickness and hole diameter.

Acknowledgements

The authors wish to thank S. Riekehr and R. Dinse from Helmholtz-Zentrum Geesthacht for their valuable support in carrying out laser shock peening experiments and L. Moura for helping with hole drilling measurements.

Declaration of conflicting interests

The authors declare that there is no conflict of interest.

Funding

This research received no specific grant from any funding agency in the public, commercial, or not-for-profit sectors.

References

1. Schajer G. Measurement of Non-Uniform Residual Stresses Using the Hole-Drilling Method. Part 1 – Stress Calculation Procedures. *J Eng Mater-T ASME* 1988; 110: 338-343.
2. Schajer G. Measurement of Non-Uniform Residual Stresses Using the Hole-Drilling Method. Part 2 – Practical Application of the Integral Method. *J Eng Mater-T ASME* 1988; 110: 334-349.
3. Schajer G. *Hole-drilling and ring core methods*, Lilburn: Fairmont Press, 1996, pp.5–20.
4. Lord J, Re Grant P, Whitehead P. *The measurement of residual stresses by the incremental hole drilling technique*. Measurement Good Practice Guide No.53. National Physical Laboratory, Teddington, 2002.
5. Beaney E M. Accurate measurement of residual stress on any steel using the centre hole drilling. *Strain* 1976; 12(3): 99-106.
6. Diaz F, Kaufmann G and Galizzi G. Determination of Residual Stresses Using Hole Drilling and Digital Speckle Pattern Interferometry with Automated Data Analysis. *Opt Lasers Eng* 2000; 33: 39–48.
7. Schajer G, Gazzarri J. Surface profiling using sequential sampling and inverse methods. Part I Mathematical background. *J Exp Mech* 2004; 44(5): 473–486.
8. Schajer G and Steinzig M. Full-field Calculation of Hole Drilling Residual Stresses from Electronic Speckle Pattern Interferometry Data. *J Exp Mech* 2005; 45(6): 526-532.
9. Beghini M, Bertini L and Santus C. A procedure for evaluating high residual stresses using the blind hole drilling method, including the effect of the plasticity. *J Strain Anal Eng* 2010; 45: 301-318.
10. Cloud G. *Optical Methods of Engineering Analysis*, Cambridge: Cambridge University Press, 1995.
11. McDonach A, McKelvie J, MacKenzie P et al. Improved Moire Interferometry and Applications in Fracture Mechanics, Residual Stress and Damaged Composites. *Exp Tech* 1983; 7: 20–24.
12. Ya M, Miao H, Zhang X et al. Determination of residual stress by use of phase shifting Moiré interferometry and hole-drilling method. *Opt Lasers Eng* 2006; 44(1): 68–79.
13. Antonov A. Inspecting the Level of Residual Stresses in Welded Joints by Laser Interferometry. *Welding Prod* 1983; 30: 29–31.
14. Jones R and Wykes C. *Holographic and Speckle Interferometry*, 2nd ed. Cambridge: Cambridge University Press, 1989.
15. Schajer G. Application of Finite Element Calculations to Residual Stress Measurements. *J Eng Mater-T ASME* 1981; 103: 157-163.
16. Seifi R and Salimi-Majd D. Effect of plasticity on residual stresses measurement by hole drilling method. *Mech Mat* 2012; 53: 72-79.

17. R Moharami and I Sattari-Far. Experimental and numerical study of measuring high welding residual stresses by using the blind-hole-drilling technique. *J Strain Anal Eng* 2007; 43:141.
18. G Li, B Liu and B Li. Influence of the hole-side plastic deformation as a result of the stress concentration on the accuracy of residual welding stress measurement by small blind hole relaxation method and its modification. In: *International conference on welding for challenging environments*, 1986.
19. Chupakhin S, Kashaev N and Huber N. Effect of elasto-plastic material behaviour on determination of residual stress profiles using the hole drilling method, *J Strain Anal Eng Des* 2016; DOI: 10.1177/0309324716663940.
20. Clauer A. Laser Shock Peening as a Surface Enhancement Process. *Key Eng Mater* 2001; 197: 121–144.
21. Rubio-Gonzales C, Felix-Martinez C, Ocana J et al. Effect of Laser Shock Processing on Fatigue Crack Growth of Duplex Stainless Steel. *Mater Sci Eng A* 2011; 528(3): 914–919.
22. Haykin S. *A comprehensive Foundation*, 2nd ed. New York: Pearson, 1998.
23. Huber N, Tsakmakis Ch. A neural network tool for identifying the material parameters of a finite deformation viscoplasticity model with static recovery, *Comput Methods Appl Mech Eng* 2001; 191: 353-384.
24. Dassault Systèmes. ABAQUS 6.13 CAE user's manual, 2013.
25. Lutz M. Learning Python, 4th ed. O'Reilly Media, 2009, p.1216.
26. ASM Aerospace Specification Metals Inc. Aluminium 2024-T3, http://asm.matweb.com/search/SpecificMaterial.asp?bassnum=MA2024T3 (2007, accessed on 07.14.2015).
27. Zainul H, Taib N and Zaharinie T. Characterization of 2024-T3: An aerospace aluminum alloy. *Mater Chem Phys* 2009; 113: 515-517.
28. Garmo P, Black J and Kohser R. *Materials and Processes in Manufacturing*, New York: John Wiley Publications, 2003.
29. Kacer H, Atik E and Miric C. *Mater Process Technol*, 2003; 142(3): 762.
30. Enz J, Khomenko V, Riekehr S and at el. Single-sided laser beam welding of a dissimilar AA2024–AA7050 T-joint. *Mater Des* 2015; 76: 110–116.
31. McClug R. Literature Survey on the Stability and Significance of Residual Stresses During Fatigue. *Fatigue Fract Engng Mater Struct* 2007; 30(3): 173–205.
32. Ding K and Ye L. *Laser Shock Peening: Performance and Process Simulation*. Cambridge: Woodhead Publishing Limited, 2006.
33. Spanrad S and Tong J. Characterisation of Foreign Object Damage (FOD) and Early Fatigue Crack Growth in Laser Shock Peened Ti-6Al-4V Aerofoil Specimens. *Mater Sci Eng A* 2011; 528(4–5): 2128–2136.

34. Correa C, Ruiz de Lara L, Diaz M et al. Effect of advancing direction on fatigue life of 316L stainless steel specimens treated by double-sided laser shock peening. *Int J Fatigue* 2015; 107: 98-107.
35. Spradlin T. *Process Sequencing for Fatigue Life Extension of Large Scale Laser Peened Components*. PhD Thesis, Wright State University, USA, 2011.
36. Ivetic G, Meneghin I, Ocana M et al. Fatigue in Laser Shock Peened Open-Hole Thin Aluminium Specimens. *Mater Sci Eng A* 2012; 534: 573–579.
37. Sano Y, Adachi T, Akita K et al. Enhancement of Surface Property by Low-Energy Laser Peening Without Protective Coating. *J Key Eng Mater* 2007; 345(3): 345–346, 1589–1592.
38. Steinzig M and Ponslet E. Residual stress measurement using the hole drilling method and laser speckle interferometry: Part 1. *Exp Tech* 2003; May/June: 43–46.
39. MSC Software. Partan user's guide, 2012.
40. Yagawa G, Okuda H. Neural networks in computational mechanics, *Arch Comput Method E* 1996; 3:435-512.
41. Willumeit R, Feyerabend F and Huber N. Magnesium degradation as determined by artificial neural networks. *Acta Biomat* 2013; 9(10): 8722-8729.
42. Huber N, Tsakmakis Ch. Determination of constitutive properties from spherical indentation data using neural networks, Part I: The case of pure kinematic hardening. *J Mech Phys Solids* 1999; 47 (7): 1569-1588.
43. Huber N, Tsakmakis Ch. Determination of constitutive properties from spherical indentation data using neural networks, Part II: Plasticity with nonlinear isotropic and kinematic hardening. *J Mech Phys Solids* 1999; 47 (7): 1589-1607.
44. Huber N, Tsagrakis I, Tsakmakis Ch. Determination of constitutive properties of thin metallic films on substrates by spherical indentation using neural networks. *Int J Solids Struct*, 2000; 37 (44): 6499-6516.
45. Huber N, Konstantinidis A, Tsakmakis Ch. Determination of Poisson‘s ratio by spherical indentation using neural networks: Part I: Theory. *J Appl Mech* 2001; 68: 218-223.
46. Huber N, Tsakmakis Ch. Determination of Poisson‘s ratio by spherical indentation using neural networks. Part II: Identification method. *J Appl Mech* 2001; 68: 224-229.
47. Huber N, Tsakmakis Ch. A neural network tool for identifying the material parameters of a finite deformation viscoplasticity model with static recovery. *Comput Methods Appl Mech Eng* 2001; 191: 353-384.
48. Huber N, Nix W, Gao H. Identification of elastic-plastic material parameters from pyramidal indentation of thin films. *Proc R Soc Lond A Math Phys Sci*, 2002; 458: 1593-1620.
49. Tyulyukovskiy E, Huber N. Identification of viscoplastic material parameters from spherical indentation data. Part I: Neural networks. *J Mater Res* 2006; 21: 664-676.

50. Schajer G, Abraham C. Residual stress measurement in finite-thickness materials by hole-drilling. *Exp Mech* 2014; 54(9): 1515.
51. ASTM E837 – 13a:2013. Standard test method for determining residual stresses by hole drilling strain gage method.